Vectorial finite difference scheme for isotropic dielectric waveguides: transverse electric field representation

A.P. Ansbro
I. Montrosset

Abstract: A computer program is demonstrated for calculating the two-dimensional transversal vectorial field in longitudinally invariant isotropic optical waveguides by applying a simple finite difference approach using successive overrelaxation on a Gauss–Seidel algorithm and estimation of the propagation constant using the Rayleigh quotient. The method is formulated in terms of the transverse electric field that implicitly satisfies the boundary conditions to the order of the discretisation step. The implementation is such that it allows the computations, even of structures with complex refractive index, to be performed on a personal computer. Using this implementation technique (based on successively more accurate approximations of the field), the first few higher order modes can be obtained without difficulty, which is usually one of the problems with this method. The comparison of results is given for standard passive structures examined and for waveguides in the index gain guiding regime.

1 Introduction

The advent of improved growth and etching techniques means that the design of microwave and optical integrated structures can be well controlled. As the fabrication of such structures becomes more precise, accurate mathematical modelling becomes increasingly more important in the design procedure. There exist many well formulated methods such as finite elements (FE) [1, 2], effective index (EI) [3, 4], spectral methods (SM) [4, 5] and finite difference (FD) [6–15], which, for a large range of optical and microwave devices, many of the procedures are adequate. This paper addresses the question of obtaining a broadly applicable algorithm, at the expense of computing time and, to some extent, memory requirement. Although it will be demonstrated that the computing time depends very strongly on the ability to generate a good initial approximation to the field and, if achieved, the computational time is, in most situations, not a limitation on the method.

For a generally applicable algorithm, it is widely recognised that an FD formulation is the one of the most robust. Often, when applied, the scalar equation is adopted [6–8] and, with a polarisation correction term added [9], or, as in the case of Stern [10–12], a semi-vectorial method (SVFD) is used. Also, it is well known that spurious modes occur when the problem is posed without the explicit satisfaction of Gauss's equation [7, 13, 14], a phenomenon occurring also in FE methods. The spurious mode fields can be circumvented by considering directly the transverse field components which implicitly satisfy $\nabla(\varepsilon E) = 0$, and this has been considered by several authors using either the transverse E or H field representation [11, 15]. However, as will be shown, it is more advantageous to use the transverse E field components because implicit satisfaction of the boundary conditions occurs to the order of the discretisation step.

In Section 2 a derivation of the transverse field equations is given and a solution method using Gauss–Seidel successive over relaxation (SOR) [16] with the Rayleigh quotient (RQ) [17] are discussed. The RQ is used for the evaluation of the propagation constant and as a measure of the convergence of the scheme. It must be noted that this is not a RQ iteration [16] scheme, but rather a hybrid form which reduces memory requirement, a feature which is discussed in more detail in Section 3. The transverse electric field equations have been reduced in complexity to generate initial fields for the vectorial equation; these being a finite difference effective index solution (EIFD) and a semivectorial finite difference solution (SVFD) which is similar to that calculated [10]. This determination of the initial field, by applying successively more accurate approximations to the vectorial equation, permits a greater control over the convergence of the relaxation algorithm allowing higher order modes to be analysed.

Section 3 deals briefly with the transformation into the appropriate FD equations, the corresponding properties, simple memory saving techniques and simple numerical implementation.

In Section 4 we compare our results with standard passive structures studied in the literature; for the one-dimensional structures of Vassallo [18] and the two-dimensional environments examined in the COST [19]

project for EIFD, SVFD and vectorial finite difference (VFD). A comparison is also made for the asymmetric filter [20–22] in which we are able to demonstrate the ability to obtain higher order modes even in strongly asymmetrical structures by using, good initial field and propagation constant approximations, a shifting theorem [16], and a low overrelaxation parameter. These results show that, contrary to Reference 10, it is possible to generate higher order eigensolutions although as stated [10] the lowest order mode is always the most stable.

The configuration considered in the final part of Section 4 is the gain guided device discussed [23] for both the quasi-TE and quasi-TM of operation, and we compare EIFD and VFD calculations of quasi-TE and quasi-TM modal gain; the EIFD results are essentially the same as those obtained [22] in which they applied a complex root searching EI method.

2 Formulation

Manipulating Maxwell's equations in the standard way, one can obtain

$$\nabla^2 E + \mu_0 \omega^2 \varepsilon E = \nabla(\nabla E) \qquad (1)$$

where μ_0 is the permeability in free space, ε is the permittivity, and the field has an angular frequency ω. The horizontal direction is denoted by x, with the y coordinate conforming to the right-handed coordinate system definition. It is possible to represent the transverse part of eqn. 1 in the form

$$\nabla_t^2 E^t + \mu \omega^2 \varepsilon E^t = \nabla_t\left(\nabla_t E^t + \frac{\partial E^z}{\partial z}\right) \qquad (2)$$

where the subscript and superscript t represent the transverse part of the operator and field $E^t = (E^x, E^y)$, respectively. The longitudinal E_z component can be eliminated by applying Gauss's equation. In making this substitution, we satisfy the divergence relation which should suppress the spurious mode solutions [7]. Applying this substitution eqn. 2 becomes

$$\partial^{\prime t}\left[\begin{pmatrix} \partial_y & -\partial_x \\ -\partial_y & \partial_x \end{pmatrix} E^t\right] + \partial^t\left[\frac{\partial^t(\varepsilon E^t)}{\varepsilon}\right]$$
$$+ (\omega^2 \mu_0 \varepsilon - \beta^2) E^t = 0 \qquad (3)$$

where an obvious differential form notation has been used to represent the partial differentials, $\partial^t = (\partial_x, \partial_y)$, $\partial^{\prime t} = (\partial_y, \partial_x)$, and β is the longitudinal propagation constant. To facilitate further discussion, eqn. 3 can be rewritten explicitly as

$$\partial_y^2 E^x + \partial_x\left[\frac{\partial_x D^x}{\varepsilon}\right] + (\mu \omega^2 \varepsilon - \beta^2) E^x$$

$$= \partial_y \partial_x E^y - \partial_x\left[\frac{\partial_y D^y}{\varepsilon}\right]$$

$$\partial_x^2 E^y + \partial_y\left[\frac{\partial_y D^y}{\varepsilon}\right] + (\mu \omega^2 \varepsilon - \beta^2) E^y$$

$$= \partial_x \partial_y E^x + \partial_y\left[\frac{\partial_x D^x}{\varepsilon}\right] \qquad (4)$$

where $D = \varepsilon$, $E = (D^x, D^y)$. Eqns. 4 are a system of coupled equations in which the left-hand sides of the equations represent the coupling of one E-polarisation to the other. The solutions of the two independent eqns. 4, with the left-hand sides equal to zero, are the quasi-TE

$(E^y = 0)$ and quasi-TM $(E^x = 0)$ fields which are similar to the semivectorial representation of Stern [10]. For this reason, when the left-hand side of eqn. 4 is zero, we call this method the semivectorial finite difference method (SVFD).

The solution scheme is based on the Gauss–Seidel [16] method used in conjunction with successive overrelaxation (SOR) [16] and employing Chebyshev acceleration [16], with β estimated using the following Rayleigh quotient formula (RQ) [16]:

$$\beta^2 = $$

$$\frac{\iint \left\{ \partial^{\prime t}\left[\begin{pmatrix} \partial_y & -\partial_x \\ -\partial_y & \partial_x \end{pmatrix} E^t\right] + \partial^t\left[\frac{\partial^t(\varepsilon E^t)}{\varepsilon}\right] + k_0^2 \varepsilon E^t \right\} E^{*t}\, dS}{\iint E^t E^{*t}\, dS}$$

$$(5)$$

where $*$ represents complex conjugation and the equality sign holds when E^t is an eigensolution. In this version, we exploit a property of the RQ, based on the theorem of Forsythe and Wasow [24] for the RQ iteration scheme discussed [25], which states that, if the system matrix is diagonally dominant, the solution will converge.

The implementation procedure is straightforward. After several iterations of the SOR scheme, an estimated value of the field is obtained and, with this, a propagation constant is estimated using RQ. This new value of β is substituted into the first equation and the iteration proceeds. This sequence is followed until the change in β is less than a specified value at which point the scheme is said to have converged.

The method of solution employs a 'cascade' approach to make the program more efficient which is realised with simplifications of eqn. 4. The reduction of eqn. 4 to one dimension gives two equations whose solutions are that of the TE or the TM fields. Applying the above numerical scheme to these one-dimensional equations, one generates a finite difference effective index solution (EIFD).

It is known and it is easily observed that, using the EI approximation, the field will be discontinuous, and insertion into the full vectorial method would appear to be numerically inefficient because a further approximation, in certain circumstances, is possible (i.e. for the quasi-TM mode, the E_x field is assumed zero and for the quasi-TE mode the E_y field is assumed zero). Using these assumptions enables a reduction of the coupled system in eqn. 4 into two uncoupled equations.

The program we have developed operates in the following 'cascade' manner. The EIFD field is calculated, this facilitates the solution of the SVFD solution and then, using this, the VFD solution is obtained. This method has been adopted for essentially two reasons. The first reason is that the solution of each field type increases in complexity from EIFD to VFD and therefore the less time spent calculating the VFD field the more efficient the calculation. In iteration schemes of this type, the computational time is strongly dependent on the initial estimate of the field and β and so we generate good estimates to the field by using successively more complicated formulations, thus saving computer time, and, for higher order modes, a good estimation of both the electric field and β are necessary for convergence. Hence with this method, by controlling EIFD precisely, one can obtain the higher order modes of the structure as is demonstrated in Section 4, where in relevant cases we include the results of both EIFD and SVFD. However, as

254

stated [10], the generation of higher order modes is much more difficult than the lowest order mode.

3 The discretisation method

Employing the standard representation for the derivative:

$$\frac{d\phi(x)}{dx} = \frac{\phi(x+h) - \phi(x-h)}{2h} + O(h^2) \tag{6}$$

to the eqns. 4 yields the corresponding finite difference representation, with eqn. 7 being the finite difference form of the first eqn. 4

$$
\begin{aligned}
E^x_{x,y}&\left\{4\delta^2_x\,\delta^2_y(\mu\omega\varepsilon_{x,y} - \beta^2) - 2\delta^2_x - \delta^2_y\left[\frac{\varepsilon_{x,y}}{\varepsilon_{x-\delta x,y}} + \frac{\varepsilon_{x,y}}{\varepsilon_{x+\delta x,y}}\right]\right\}\\
&+ \delta^2_x(E^x_{x,y+2\delta y} + E^x_{x,y-2\delta y})\\
&+ \delta^2_y\left(E^x_{x+2\delta x,y}\left\{\frac{\varepsilon_{x+2\delta x,y}}{\varepsilon_{x+\delta x,y}}\right\} + E^x_{x-2\delta x,y}\left\{\frac{\varepsilon_{x-2\delta x,y}}{\varepsilon_{x-\delta x,y}}\right\}\right)\\
&+ \delta_x\,\delta_y\left(E^y_{x+(1+a)\delta x,\,y+\delta y}\frac{\varepsilon_{x+(1+a)\delta x,\,y+\delta y}}{\varepsilon_{x+(1+a)\delta x,\,y}}\right.\\
&\qquad - E^y_{x+(1+a)\delta x,\,y-\delta y}\frac{\varepsilon_{x+(1+a)\delta x,\,y-\delta y}}{\varepsilon_{x+(1+a)\delta x,\,y}}\Bigg)\\
&+ \delta_x\,\delta_y\left(E^y_{x-(1-a)\delta x,\,y-\delta y}\frac{\varepsilon_{x-(1-a)\delta x,\,y-\delta y}}{\varepsilon_{x-(1-a)\delta x,\,y}}\right.\\
&\qquad - E^y_{x-(1-a)\delta x,\,y+\delta y}\frac{\varepsilon_{x-(1-a)\delta x,\,y+\delta y}}{\varepsilon_{x-(1-a)\delta x,\,y}}\Bigg)\\
&- \delta_x\,\delta_y(E^y_{x+\delta x,\,y+(1+b)\delta y} - E^y_{x+\delta x,\,y-(1-b)\delta y}\\
&\qquad + E^y_{x-\delta x,\,y-(1-b)\delta y} - E^y_{x-\delta x,\,y+(1+b)\delta y})\\
&= 0
\end{aligned}\tag{7}
$$

and obtaining the second eqn. (4) by the interchanging of x and y and a and b. The variables a and b are equal to 0 when there is no discontinuity in refractive index. If the discontinuity is in the x direction, a takes the value of 2 or -2 depending on the position of the discontinuity; the same rules apply to b when there is a discontinuity in the y direction. The mathematical details concerning continuity and satisfaction of the boundary conditions are discussed in Appendix 7.

The mesh is constructed so that the discontinuities lie between index discretisation points and that there are at least three field points in any given layer or the change in index over three field points is less than the order of the discretisation step.

The memory saving advantage of this difference scheme can be seen when the E_y field points are shifted by $(\delta x, \delta y)$ wrt the E_x field points as is shown in Fig. 1. In Fig. 1 the positions of all the necessary field points are shown for the determination of the two field points indicated, and it can be seen that both E_x and E_y field points are each spaced by twice the discretisation step. Thus eqn. 7 can be satisfied by considering only field points spaced twice the discretisation step apart and located in the manner depicted in Fig. 1 (i.e. evaluating E_x and E_y at adjacent mesh points). Therefore this scheme requires only one-eighth of the memory requirement needed to represent the vectorial field at each mesh point but it still evaluates eqn. 7 to the same order of discretisation error. The discretisation of the refractive index profile is assumed constant in rectangular sections as indicated in Fig. 1.

In many structures the dimensions are such that it is preferable to have a FD mesh which is nonuniform. Our program has been adapted so that a nonuniform mesh is possible in the vertical direction (y), while maintaining
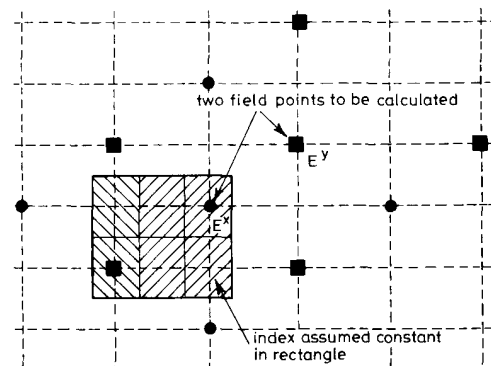

Fig. 1 *Homogeneous FD mesh*

● and ■ represent positions of where E^x and E^y are computed, intersections of dotted lines indicate refractive index mesh

the properties mentioned previously; those of memory saving and implicit boundary condition satisfaction to the order of the size of the discretisation step. Two restrictions are imposed on the grid points; the first is that the interface between adjacent regions with different y discretisation must be in a region where there is no change in the refractive index in the y direction. The second restriction is that the change in mesh size from one section to another can be only 0.5 or 2 times that of the adjacent meshes. These are purely arbitrary restrictions on the formation of the mesh but they enable the determination of field points in a simple manner. A typical interface between meshes is shown in Fig. 2 and
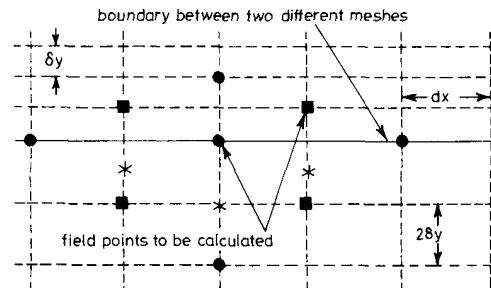

Fig. 2 *FD grid at boundary between different y discretisation steps*
* indicate extra field points which must be evaluated

that the actual calculated field points and positions are shown in same manner as in Fig. 1. However, to evaluate the field points indicated it is necessary to evaluate the field at the points indicated with *, the reason for which can easily be seen by comparing with Fig. 1. The calculation of the fields at positions * is by linear interpolation of the nearest appropriate field points.

If the nonuniform mesh is introduced, it is possible to have a significant saving in memory requirement without loss of accuracy. For example, in the COST structures, there was agreement in the first five digits of β between a nonuniform mesh (60 field points in the y direction) and a

uniform mesh (114 field points) with the smallest discretisation step in the nonuniform mesh being equal to the discretisation in the uniform case ($\delta y = 0.02$ μm). The discretisation in the x direction was 0.1 μm. It is difficult to implement criteria that can determine when the finite size of the finite difference mesh does not influence the calculation of b; from our experience, when the field lines (30 dB down on the maximum field value) are not influenced greatly by the box, there is a negligible difference in the b values.

When implementing this finite difference scheme, together with the Gauss–Seidel successive overrelaxation algorithm, the memory requirement is less than that needed for standard matrix inversion methods, and thus allows the calculation of modal fields in complex refractive index environments to be performed on a personal computer.

4 Results and comparisons

All results in this Section were calculated using a 386 (33 MHz) personal computer, and the approximate CPU time for each structure, together with the appropriate discretisation size, is included where relevant.

We first consider the 1D structures examined by Vassallo [18]. In Fig. 3 the simple slab structure is modelled
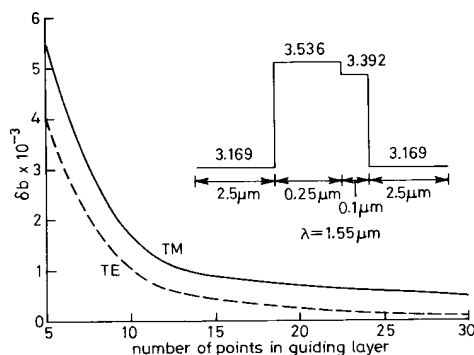

Fig. 3 *Convergence properties of FD scheme for weakly asymmetric 1D waveguide* [18]

and $\delta b = b - b_{exact}$ is calculated as a function of the number of points in the guiding layer. Here b is defined in the usual way; $b = (n_{eff}^2 - n_s^2)/(n_g^2 - n_s^2)$, where n_{eff} is the effective index of the mode, and n_g and n_s are the indices of the guide and substrate, respectively. The 'exact' value b_{exact} is evaluated by searching of the zero of the transverse resonance condition for the structure. The size of the interval used for the finite difference procedure is constructed from the criterium discussed in Section 3. Fig. 3 demonstrates the convergence of both the TE and TM solutions as the discretisation step is decreased. The size of the discretisation step required for $\delta b < 10^{-3}$ is approximately the same as that found by Vassallo [18] (i.e. 10 field points in the guiding layer).

The second 1D structure of Vassallo is shown in Fig. 4, together with the convergence properties, as a function of the number of points in the interval of 7.5 μm. For the TE case we have used a uniform mesh and for the TM case a nonuniform mesh. The nonuniform mesh is required for the TM field because, at the boundary between the guiding layer and the air, the E field varies faster than in the TE case. To maintain accurate satisfaction of the boundary conditions, we must therefore

increase the number of points near this interface. The nonuniform scheme is represented in Fig. 4 in which we require many more points than Vassallo in the guiding layer. However, the total number of points required over the entire interval is only approximately 30% greater.
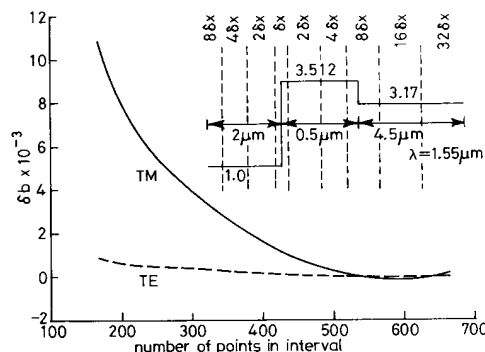

Fig. 4 *Convergence properties of FD scheme for strongly asymmetric 1D waveguide* [18]

nonuniform mesh is shown explicitly in insert

The first 2D structure that we investigate is that of COST [19]; the results for our three methods (EIFD, SVFD, and VFD) are given in Table 1 with the COST

Table 1: Comparison of b values of COST [19], Stern [10] and our technique for COST [19] structure

d	EI	EIFD	SV	SVFD	VFD	VFD
μm	COST	Our	Stern	Our	COST	Our
TE						
0.0	0.1380	0.1362	0.1181	0.1170	0.1161	0.1175
0.2	0.1431	0.1428	0.1354	0.1342	0.1322	0.1367
0.4	0.1542	0.1542	0.1511	0.1517	0.1478	0.1517
TM						
0.0	0.1113	0.1061	0.0911	0.0873	—	0.0876
0.2	0.1118	0.1093	0.1030	0.1045	—	0.1052
0.4	0.1207	0.1194	0.1170	0.1170	—	0.1175

results and those of Stern [10] for his SVFD. The parameter d is the thickness of the layer between the guiding layer and the air–dielectric interface. There are no results for the quasi-TM field [19] for the single rib structure calculated by a VFD.

The discrepancies in the EI and the EIFD are greatest when $d = 0$ which is due to the fact that, in the region where there is no rib, the slab structure cannot support a guided mode and consequently [19], and in our EIFD, a different effective index is assumed in this region. The rest of results show good agreement with Stern [10] and COST [19], the differences could be attributed to the size of the area enclosed by the FD mesh and to the different numerical procedures employed.

The results in Table 2 are for the coupled structure [19] in which the two guides have the same geometry as in the single rib case with $d = 0.4$ μm and the separation distance between guides is S [μm]. Unfortunately there is no VFD solution for the directional coupler in the COST project and therefore a set of VFE results is given as a reference. The coupling length L_c is calculated in the normal way by $L_c = 0.5\lambda/(n_s/n_{as})$ where λ is the operating wavelength and n_s and n_{as} are the effective indices of the symmetric and antisymmetric mode, respectively.

The FD mesh for these structures was $\delta x = 0.05$ μm and the minimum value of the y discretisation was

Table 2: Coupling length in mm for COST [19] directional coupler

S	EI	EIFD	SV	SVFD	VFEM	VFD
μm	COST	Our	Stern	Our	COST	Our
TE						
0	0.147	0.145	0.130	0.131	0.135	0.135
1	0.309	0.310	0.337	0.343	0.342	0.345
2	0.656	0.662	0.669	0.680	0.677	0.685
3	1.39	1.36	1.31	1.29	1.33	1.29
4	2.92	2.80	2.53	2.58	2.59	2.58
TM						
0	0.124	0.119	0.113	0.112	0.112	0.114
1	0.324	0.330	0.381	0.360	0.369	0.375
2	0.855	0.866	0.958	0.920	0.941	0.935
3	2.25	2.31	2.39	2.00	2.57	2.18
4	5.93	6.21	5.90	5.76	6.41	6.04

$\delta y = 0.02\ \mu m$. The CPU time required to obtain the COST solutions was less than 2 minutes.

Now we examine the asymmetric coupler used as a filter discussed [20–22], which demonstrates the ability of this scheme to generate the second mode solution for a weakly coupled and strongly asymmetric structure that can be calculated without any difficulty in convergence. The coupling length for the quasi-TE mode in the structure depicted in Fig. 5 at an operating wavelength of
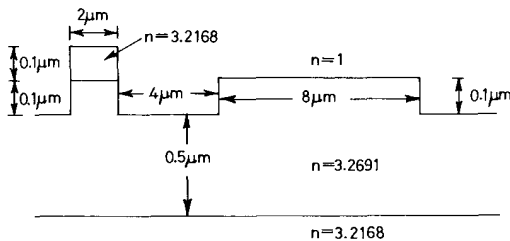
Fig. 5 *Directional coupler band pass filter* [20]
Operating wavelength = 1.2663 microns

$1.2663\ \mu m$ is 11 mm using our technique, while in References 20 and 21 is 14 mm. This difference in coupling length corresponds to a difference of 1.3×10^{-5} in the calculation of $n_s - n_{as}$; an important fact which must be borne in mind when considering coupling lengths in weakly coupled regimes. The weakly coupled nature of the first two modes of the structure is evident in Fig. 6, with the contour levels equally spaced between the maximum value and the minimum value of the field. To obtain the appropriate accuracy for the coupling length for these types of weakly coupled structures, it is better transferred to a mainframe computer or to use the spectral index (SI) method [21, 22] which is better suited to this type of calculation using a personal computer. Similar structures [20–22] are studied by Benson [26] and our quasi-TE results compare favourably.

The mesh for these structures was $\delta y = 0.01\ \mu m$ and $\delta x = 0.1\ \mu m$ and the CPU time requirement was approximately 4 minutes.

The final structure that we consider is a ridge waveguide (Fig. 7a) operating in the gain guided regime in which we wish to evaluate the modal gain for quasi-TE and quasi-TM modes, which are necessary in the design of optical polarisation insensitive ridge waveguide amplifiers [23].

In Reference 23 the variation of the refractive index in the active layer was calculated from the carrier distribution which is, itself, obtained from the solution of the dif-

fusion equation; a typical refractive index profile in the active layer is shown in Fig. 7b. In our calculation we wish to determine whether the condition of equal quasi-TE and quasi-TM modal gain is the same for both the EI method [23] and our VFD method.
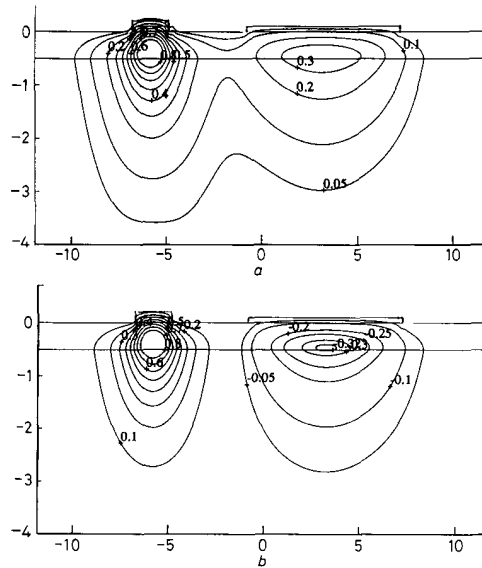
Fig. 6 E_x *field contours of modes of directional coupler band pass filter in Fig. 5*
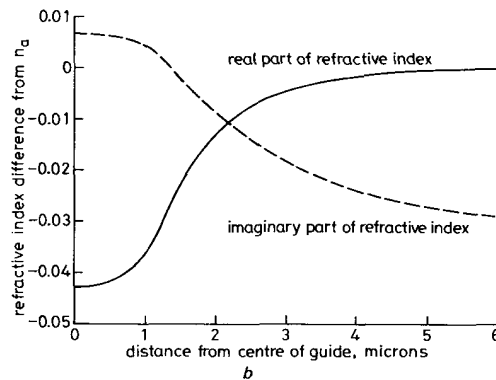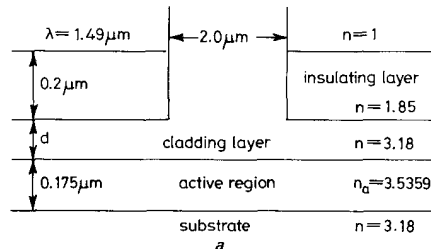a Symmetric
b Antisymmetric

Fig. 7 (a) *Configuration of ridge waveguide laser amplifier* [23]; (b) *Typical real and imaginary refractive index variation in active layer produced by current injection*

In Fig. 8 the behaviour of the quasi-TE and quasi-TM modal gain, calculated by the EIFD and the VFD, is shown as a function of the cladding layer thickness (d).

The evaluation of modal gain for the device in Fig. 8 operating at a wavelength $\lambda = 1.49\ \mu m$ and 100 μm long is $4.343 \times 100 \times 2 \times \mathrm{Im}\ \{\beta_i\}$ dB, where β_i is the propaga-
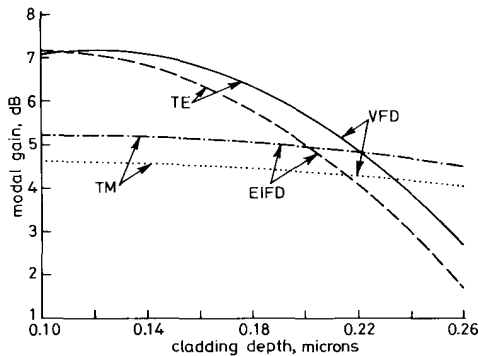

Fig. 8 *Modal gain of quasi-TE and quasi-TM modes as function of cladding layer thickness (d in Fig. 7a)*

$\lambda = 1.49$ microns
——— TE gain by VFD
– – – – TE gain by EIFD
········· TM gain by VFD
—·—· TM gain by EIFD

tion constant for the mode and the maximum concentration of injected carriers is $3.2 \times 10^{18}\ cm^{-3}$. The cladding layer thickness for equal TE and TM modal gain is calculated by EIFD as $0.205\ \mu m$ with a modal gain of 4.3 dB, whereas, when calculated by VFD, the cladding layer depth is $0.235\ \mu m$ and the gain is 4.9 dB.

In this case the computational time is increased owing to the complex nature of the refractive index; it was approximately 15 minutes on a PC for a mesh $\delta y = 0.00875\ \mu m$ and $\delta x = 0.02\ \mu m$. This type of calculation is obviously better transferred to a mainframe computer.

5   Conclusions

In this paper we have demonstrated a simple vectorial finite difference scheme based on transverse representation of the electric field. The solution technique is a finite difference algorithm employing Gauss–Seidel successive overrelaxation and an estimate of the propagation constant via the Rayleigh quotient expression. As most of the optical devices of interest are fabricated in planar structures, the program has a nonuniform distribution of field points in the vertical direction to decrease memory requirement. The solution method is such that it is possible to obtain higher order modes by using successively more accurate approximations to the vectorial equation and this has been demonstrated in examination of the coupling length of a directional coupler filter [20].

This method gives good agreement with the literature when comparing relevant quantities. The method has also been applied to the more complicated case in which a structure has both gain and loss; the ridge waveguide amplifier [23].

6   References

1 RAHMAN, B.M.A., and DAVIE, J.B.: 'Finite element analysis of optical and microwave waveguide problems', *IEEE Trans.*, 1984, **MTT-32**, pp. 20–28
2 BABUSKA, I., ZIENKIEWICZ, O.C., GAGO, J., and DE A. OLIVEIRA, E.R.: 'Accuracy, estimates, and adaptive refinements in finite element computations' (John Wiley and Sons, 1986)

3 ARIV, Y.: 'Introduction to optical electronic' (Holt-Reinhard, New York, 1976)
4 BENSON, T.M., BOZEAT, P.J., and KENDALL, P.C.: 'Rigorous effective index method for semiconductor rib waveguides', *IEE Proc. J*, 1992, **139**, (1), pp. 67–70
5 ITOH, T., and MITTRA, R.: 'Spectral-domain approach for calculating the dispersion characteristics of microstrip lines', *IEEE Trans.*, 1973, **MTT-21**, pp. 496–499
6 MAO, Z., and HUANG, W.-P.: 'Analysis of optical rib waveguides and couplers with buried guiding layer', *IEEE J.*, 1992, **QE-28**, (1), pp. 176–183
7 SCHULZ, N., BIERWIRTH, K., and ARNDT, F.: 'Rigorous finite-difference analysis of coupled channel waveguides with arbitrarily varying index profile', *J. Lightwave Technol.*, 1991, **9**, (10), pp. 1244–1253
8 SEKI, S., YAMANAKA, T., and YOKOYAMA, K.: 'Two-dimensional analysis of optical waveguides with a nonuniform finite difference method', *IEE Proc. J*, 1991, **138**, (2), pp. 123–127
9 BENSON, T.M., KENDALL, P.C., MATIN, M.A., and STERN, M.S.: 'Polarisation correction applied to scalar analysis of semiconductor rib waveguide', *IEE Proc. J*, 1992, **139**, (1), pp. 39–41
10 STERN, M.S.: 'Rayleigh quotient solution of semivectorial field problems for optical waveguides with arbitrary index profiles', *IEE Proc. J*, 1991, **138**, (3), pp. 185–190
11 STERN, M.S.: 'Semivectorial polarised finite difference method for optical waveguides with arbitrary index profiles', *IEE Proc. J*, 1988, **135**, (1), pp. 56–63
12 STERN, M.S.: 'Semivectorial polarised H field solutions for dielectric waveguides with arbitrary index profiles', *IEE Proc. J*, 1988, **135**, (5), pp. 333–338
13 CORR, D.G., and DAVIS, J.B.: 'Computer analysis of the fundamental and higher order modes in single and coupled microstrip', *IEEE Trans.*, 1972, **MTT-20**, (10), pp. 669–677
14 SCHWEIG, E., and BRIDGES, W.B.: 'Computer analysis of dielectric waveguides: a finite-difference method', *IEEE Trans.*, 1984, **MTT-32**, (5), pp. 531–541
15 GELDER, D.: 'Numerical determination of microstrip properties using the transverse field components', *Proc. IEE*, 1970, **117**, (4), pp. 699–703
16 BATHE, K.-J.: 'Finite element procedures in engineering analysis' (Prentice-Hall, Englewood Cliffs, New Jersey, 1982)
17 PARLETT, B.N.: 'The symmetric eigenvalue problem' (Prentice-Hall series in computing mathematics, 1980)
18 VASSALLO, C.: 'Improvement of finite difference methods for step-index optical waveguides', *IEE Proc. J*, 1992, **139**, (2), pp. 137–142
19 WORKING GROUP 1, COST 216: 'Comparison of different modelling techniques for longitudinally invariant integrated optical waveguides', *IEE Proc. J*, 1989, **136**, (5), pp. 273–280
20 BURKE, S.V., KENDALL, P.C., RITCHIE, S., ROBERTSON, M.J., and ROBSON, P.N.: 'Analysis of rib waveguide coupler filters', *IEE Proc. J*, 1992, **139**, (1), pp. 59–65
21 BURKE, S.V.: 'Analysis of a novel rib waveguide wavelength filter by the spectral index method', in 'Technical digest on integrated photonics research' (Optical Society of America, Washington, DC, 1990), Vol. 5, pp. 86–87
22 ROBSON, P., and KENDALL, P.: 'Rib waveguide analysis by the spectral index method' (Research Studies Press, John Wiley, 1990), pp. 148–149
23 GOANO, M., MAIO, I., and MONTROSSET, I.: 'Design of high power low noise polarisation insensitive ridge waveguide laser amplifiers', *J. Lightwave Technol.*, in press
24 FORSYTHE, G.E., and WASOW, W.R.: 'Finite difference methods for partial differential equations' (Wiley, New York, 1960), Chaps. 21–22
25 HORNSBY, J.S., and GOPINATH, A.: 'Numerical analysis of a dielectric-loaded waveguide with a microstrip line-finite-difference methods', *IEEE Trans.*, 1969, **MTT-17**, (9), pp. 684–690
26 BENSON, T.M., and KENDALL, P.C.: 'Equipartition method for the analysis of two non-identical closely separated rib waveguides', *IEE Proc. J*, 1993, **140**, (1), pp. 62–65

7   Appendix

Eqn. 6 is valid only when the function $\phi(x)$ is continuous and its derivative exists over the desired interval. If there is a point at which $\phi(x)$ is continuous but $d_x\,\phi(x)$ is undefined, this formula cannot be strictly applied. The method that we adopt is to place the point at which the discontinuity exists between discretisation points; termed the classical formulation [18]. To explain the procedure, con-

sider the one-dimensional equations obtained from eqn. 4

$$d_y^2 E^x = (\beta^2 - \mu\omega^2\varepsilon)E^x \qquad (8)$$

$$d_y\left[\frac{d_y D^y}{\varepsilon}\right] = (\beta^2 - \mu\omega^2\varepsilon)E^y \qquad (9)$$

The solutions of eqns. 8 and 9 are the TE and TM modes in a one-dimensional structure. Eqn. 8 is essential the one-dimensional scalar wave equation because both E^x and $d_y E^x$ are continuous across dielectric interfaces. When the dielectric is a continuous function, both sides of eqn. 8 are continuous and eqn. 6 can be rigorously applied. If, however, there is a discontinuity in ε, the right-hand side (RHS) of eqn. 8 has a discontinuity, which, in turn, implies that the second derivative of E^x on the left-hand side (LHS) of eqn. 8 has the same discontinuity. This implies that $d_y E^x$ is continuous with a discontinuous change in its derivative where there is a discontinuity in ε. The finite difference eqn. 6 is applied by placing the discontinuity between index discretisation points [18].

Consider now eqn. 9, which is the exact equation for the TM field, in which we know that E^y is discontinuous and D^y is continuous when there is a discontinuity in ε. When ε is discontinuous, the second term on the RHS of eqn. 9 is continuous, but the first term is discontinuous. This implies that the term in the square brackets on the LHS of eqn. 9 is continuous with a undefined derivative corresponding to the discontinuity in ε. In this case, D^y must be continuous, but the derivative of D^y has a discontinuity which cancels the discontinuity in ε; implying that $d_y D^y/\varepsilon$ is a continuous function with an undefined derivative where ε has a discontinuity.

Thus all functions which we must differentiate are continuous but may not possess a derivative when there is a discontinuity in ε. We can therefore state that the finite difference representation of eqn. 6 can be applied to eqns. 8 and 9, and hence to all the derivatives on the LHS of eqn. 4, with the same constraint as that imposed on the scalar wave equation (i.e. Taylor's expansion of a function which does not possess a derivative at every interior point is not strictly valid and the point at which the derivative is undefined is placed halfway between index mesh points).

Consider now the discretisation of the RHS of eqn. 4. In eqn. 10, only the RHS of the first eqn. 4 is given, as

symmetrical arguments hold for the remaining terms in the second equation:

$$\partial_y(\partial_x E^y) - \partial_x\left[\frac{\partial_y(D^y)}{\varepsilon}\right] \qquad (10)$$

From the previous discussion both terms in round brackets are continuous with or without a derivative defined over the desired interval, and the application of eqn. 10 is possible.

If there is a discontinuity in ε in the y direction, the first term of eqn. 10 is discontinuous and we can represent the differential wrt y with a simple two point formula on one side of the discontinuity. There is no problem with the expansion of the second term in eqn. 11 with this discontinuity.

If the discontinuity of ε is in the x direction, the first term in eqn. 11 can be expressed using eqn. 6. The second term, however, requires that the differential wrt x is approximated from only side of the discontinuity. Using this approach, we can express the eqns. 4 using eqn. 6 as is shown in eqn. 7.

For the discussion of boundary conditions, it is useful to return to eqn. 9 and to consider the case when there is a discontinuity in the refractive index from ε^0 to ε^1 halfway between y and $y + \delta y$. Then applying eqn. 6:

$$-\varepsilon_y E_y^y\left[\frac{1}{\varepsilon_{y-\delta y}} + \frac{1}{\varepsilon_{y+\delta y}}\right] + E_{y+2\delta y}^y\left\{\frac{\varepsilon_{y+2\delta y}}{\varepsilon_{y+\delta y}}\right\}$$

$$+ E_{y-2\delta y}^y\left\{\frac{\varepsilon_{y-2\delta y}}{\varepsilon_{y-\delta y}}\right\} = O(4\delta y^2) \quad (11)$$

with the constraints detailed above $\varepsilon_{y-2\delta y} \simeq \varepsilon_{y-\delta y} \simeq \varepsilon_y \simeq \varepsilon^0$ and $\varepsilon_{y+2\delta y} \simeq \varepsilon_{y+\delta y} \simeq \varepsilon_y \simeq \varepsilon^1$. If one then expands the E field on the left of the discontinuity to the point y and the E field to the right of the discontinuity to the point $y + \delta y$, one obtains

$$\varepsilon^0 E_y^y = \varepsilon^1 E_{y+\delta y}^y + O(2\,\delta y) \qquad (12)$$

the approximate satisfaction of the boundary condition. In the limit, as step size tends to zero, the satisfaction of boundary condition is exact. Using a similar approach one can obtain without difficulty, from eqn. 4, the satisfaction of the four boundary conditions in the two-dimensional case to the order of the discretisation step.